

Complex Tire-Ground Interaction Simulation: Recent Developments Of An Advanced Shell Theory Based Tire Model

REFERENCE: Bozdog, D. and Olson, W. W., “Complex Tire-Ground Interaction Simulation: Recent Developments Of An Advanced Shell Theory Based Tire Model” submitted for presentation at the 2005 Tire Society meeting, and for consideration for publication in the journal *Tire Science and Technology*.

ABSTRACT: The formulation of an advanced shell theory based tire model (ASTBTM) provides the foundation for tire-ground interaction analysis. Micro-mechanics, composite laminate and shell theories are integrated in a consistent tire model solved by a dual symbolic-numeric algorithm. The complex tire-ground interaction is carefully examined by a sensitive numerical procedure and adaptive iteration step. Deformations and stress-strains of the entire tire structure are described as function of applied forces at the contact interface. The accuracy of solutions is found to be highly depended on mesh size, but consistent over the iterations. The elaborate theoretical model is efficiently balanced by the symbolic computation reduction technique and the system numerical optimization. Finite difference method is used extensively. Simulation provides a step-by-step insight into force generation and macroscopic behavior of the tire. The code developed provides an alternative to existing tire model implementations in vehicle dynamics simulation software.

Table of Nomenclature

p_ϕ, p_ξ, p_z – surface load components
 u, v, w – displacements components
 A, B – Lamé parameters
 A_{ij}, B_{ij}, D_{ij} – stiffness coefficients
 $K_\phi, K_\xi, K_{\phi\xi}$ - change of curvature
 $N_\phi, N_\xi, N_{\phi\xi}$ – force resultants
 $M_\phi, M_\xi, M_{\phi\xi}$ - moment resultants
 Q_ϕ, Q_ξ - shearing forces
 R_1, R_2 – radii of curvature
 $\epsilon_\phi, \epsilon_\xi, \gamma_{\phi\xi}$ - strain components
 ϕ, ξ, z – curvilinear coordinate system
 $\sigma_\phi, \sigma_\xi, \tau_{\phi\xi}$ – stress components

Introduction

The complexity of anisotropic shells of arbitrary shapes with non-symmetrical loads has generated an intense field of research for many decades. Although an exact solution for the general case does not exist, various mathematical models have brought their contribution to a general formulation of advanced tire models. This paper continues the development of an advanced shell theory based tire model [1].

Tire Model

The general system of equations defining the tire behavior is composed of compatibility, constitutive and equilibrium equations. By reducing the three dimensional carcass of the tire to two dimensions, modeling all loadings at middle surface, applying boundary conditions, and performing future simplifications, the system can be written as [2,3,4,5]:

Compatibility equations:

$$\begin{aligned}
 \varepsilon_\phi &= \frac{1}{A} \left(\frac{\partial u}{\partial \phi} \right) + \frac{1}{AB} \left(\frac{\partial A}{\partial \xi} \right) v + \frac{w}{R_1} \\
 \varepsilon_\xi &= \frac{1}{B} \left(\frac{\partial v}{\partial \xi} \right) + \frac{1}{AB} \left(\frac{\partial B}{\partial \phi} \right) u + \frac{w}{R_2} \\
 \gamma_{\phi\xi} &= \frac{B}{A} \frac{\partial}{\partial \phi} \left(\frac{v}{B} \right) + \frac{A}{B} \frac{\partial}{\partial \xi} \left(\frac{u}{A} \right) \\
 K_\phi &= \frac{1}{A} \frac{\partial}{\partial \phi} \left(\frac{u}{R_1} + \frac{1}{A} \frac{\partial w}{\partial \phi} \right) + \frac{1}{AB} \frac{\partial A}{\partial \xi} \left(\frac{v}{R_2} + \frac{1}{B} \frac{\partial w}{\partial \xi} \right) \\
 K_\xi &= \frac{1}{B} \frac{\partial}{\partial \xi} \left(\frac{v}{R_2} + \frac{1}{B} \frac{\partial w}{\partial \xi} \right) + \frac{1}{AB} \frac{\partial B}{\partial \phi} \left(\frac{u}{R_1} + \frac{1}{A} \frac{\partial w}{\partial \phi} \right) \\
 K_{\phi\xi} &= \frac{1}{AB} \left(-\frac{1}{A} \frac{\partial A}{\partial \xi} \frac{\partial w}{\partial \phi} - \frac{1}{B} \frac{\partial B}{\partial \phi} \frac{\partial w}{\partial \xi} + \frac{\partial^2 w}{\partial \phi \partial \xi} \right) - \frac{A}{BR_1} \frac{\partial}{\partial \xi} \left(\frac{u}{A} \right) - \frac{B}{AR_2} \left(\frac{v}{B} \right)
 \end{aligned} \tag{1}$$

Constitutive equations:

$$\begin{bmatrix} N_\phi \\ N_\xi \\ N_{\phi\xi} \\ M_\phi \\ M_\xi \\ M_{\phi\xi} \end{bmatrix} = \begin{bmatrix} A_{11} & A_{12} & A_{16} & B_{11} & B_{12} & B_{16} \\ A_{12} & A_{22} & A_{26} & B_{12} & B_{22} & B_{26} \\ A_{16} & A_{26} & A_{66} & B_{16} & B_{26} & B_{66} \\ B_{11} & B_{12} & B_{16} & D_{11} & D_{12} & D_{16} \\ B_{12} & B_{22} & B_{26} & D_{12} & D_{22} & D_{26} \\ B_{16} & B_{26} & B_{66} & D_{16} & D_{26} & D_{66} \end{bmatrix} \begin{bmatrix} \varepsilon_\phi \\ \varepsilon_\xi \\ \gamma_{\phi\xi} \\ K_\phi \\ K_\xi \\ K_{\phi\xi} \end{bmatrix} \tag{2}$$

Equilibrium equations:

$$\begin{aligned}
\frac{\partial}{\partial \phi}(N_{\phi}B) + \frac{\partial}{\partial \xi}(N_{\xi\phi}A) + N_{\phi\xi} \frac{\partial A}{\partial \xi} - N_{\xi} \frac{\partial B}{\partial \phi} + Q \frac{AB}{R_1} + p_{\phi}AB &= 0 \\
\frac{\partial}{\partial \xi}(N_{\xi}A) + \frac{\partial}{\partial \phi}(N_{\phi\xi}B) + N_{\xi\phi} \frac{\partial B}{\partial \phi} - N_{\phi} \frac{\partial A}{\partial \xi} + Q_{\xi} \frac{AB}{R_2} + p_{\xi}AB &= 0 \\
\frac{\partial}{\partial \phi}(Q_{\phi}B) + \frac{\partial}{\partial \xi}(Q_{\xi}A) - N_{\phi} \frac{AB}{R_1} - N_{\xi} \frac{AB}{R_2} + p_zAB &= 0 \\
\frac{\partial}{\partial \phi}(M_{\phi\xi}B) + \frac{\partial}{\partial \xi}(M_{\xi}A) - M_{\phi} \frac{\partial A}{\partial \xi} + M_{\xi\phi} \frac{\partial B}{\partial \phi} - Q_{\xi}AB &= 0 \\
\frac{\partial}{\partial \xi}(M_{\xi\phi}A) + \frac{\partial}{\partial \phi}(M_{\phi}B) - M_{\xi} \frac{\partial B}{\partial \phi} + M_{\phi\xi} \frac{\partial A}{\partial \xi} - Q_{\phi}AB &= 0 \\
N_{\phi\xi} - N_{\xi\phi} + \frac{M_{\phi\xi}}{R_1} - \frac{M_{\xi\phi}}{R_2} &= 0
\end{aligned} \tag{3}$$

Boundary conditions:

$$u(\phi, \xi) = v(\phi, \xi) = w(\phi, \xi) = 0 \tag{4}$$

There are two techniques to solve the general system of equations in terms of the displacements or in terms of the internal force and moment resultants. Both techniques require a reduction of the number of equations by substitutions and by increasing the order of the differential equations. The first method is preferred because the final system can be expressed as a system of three governing partial differential equations for displacements u , v , and w .

The first substitution replaces the strains in constitutive equations (2) with the compatibility equations (1). The force and moment resultants are now expressed as functions of displacements and their derivatives.

$$\begin{aligned}
F = f(u, v, w, \frac{\partial u}{\partial \phi}, \frac{\partial u}{\partial \xi}, \frac{\partial v}{\partial \phi}, \frac{\partial v}{\partial \xi}, \frac{\partial w}{\partial \phi}, \frac{\partial w}{\partial \xi}, \frac{\partial^2 w}{\partial \phi^2}, \frac{\partial^2 w}{\partial \xi^2}, \frac{\partial^2 w}{\partial \phi \partial \xi}, A_{ij}, B_{ij}, D_{ij}, R_1, R_2) \\
\text{for} \\
F \rightarrow \{N_{\phi}, N_{\xi}, N_{\phi\xi}, M_{\phi}, M_{\xi}, M_{\phi\xi}\} \\
i \rightarrow \{1, 2, 6\} \\
j \rightarrow \{1, 2, 6\}
\end{aligned} \tag{5}$$

The inter-ply shear forces Q_{ϕ} , Q_{ξ} are determined from the equilibrium equations (3):

$$\begin{aligned}
Q_\phi &= \frac{1}{AB} \left(\frac{\partial}{\partial \xi} (M_{\phi\xi} A) + \frac{\partial}{\partial \phi} (M_\phi B) - M_\xi \frac{\partial B}{\partial \phi} + M_{\phi\xi} \frac{\partial A}{\partial \xi} \right) \\
Q_\xi &= \frac{1}{AB} \left(\frac{\partial}{\partial \phi} (M_{\phi\xi} B) + \frac{\partial}{\partial \xi} (M_\xi A) - M_\phi \frac{\partial A}{\partial \xi} + M_{\phi\xi} \frac{\partial B}{\partial \phi} \right)
\end{aligned} \tag{6}$$

In the final substitution, the force and moment resultants and the inter-ply shear forces are replaced in the first three equilibrium equations (3). The resulting fourth-order differential system of equations relates the applied forces to the displacements. Together with the boundary conditions, the system is fully determined and finite difference method is applied.

$$\begin{aligned}
& \text{Equation} \left(u, v, w, \frac{\partial^s m}{\partial n^s}, A, B, A_{ij}, B_{ij}, D_{ij}, R_1, R_2, p_\phi, p_\xi, p_z \right)_t = 0 \\
& \text{for} \\
& t \rightarrow \{1, 2, 3\} \\
& s \rightarrow \{1, 2, 3, 4\} \\
& i \rightarrow \{1, 2, 6\} \\
& j \rightarrow \{1, 2, 6\} \\
& m \rightarrow \{N_\phi, N_\xi, N_{\phi\xi}, M_\phi, M_\xi, M_{\phi\xi}\} \\
& n \rightarrow \{\phi, \xi\}
\end{aligned} \tag{7}$$

The finite difference method is applied using the central difference scheme. The computations were performed using Mathematica™ Software.

Algorithm

For each iteration step corresponding to an increment in the applied internal and external load, the radii of the curvature and the deformed profile are computed. The overall algorithm has the following steps:

- Input profile,
- Computation of shells position,
- Find fitting functions for profile,
- Computation of curvatures, radii of curvature and Lamé parameters,
- Input stiffness matrix for composite structure,
- Symbolic computation and reduction technique for system of equations,
- Generation of complete system of equations and FDM scheme implementation,
- Input BC's and applied force matrix
- Solve system and output u , v , and w for all shell elements
- Compute all other 15 variables
- Compute deformed profile

The expression for the deformed shape computed after each iteration:

$$\begin{aligned}
 x_{k+1} &= x_k - u_{k+1} \cos(\phi) \sin(\xi) + v_{k+1} \cos(\xi) + w_{k+1} \sin(\phi) \sin(\xi) \\
 y_{k+1} &= y_k + u_{k+1} \sin(\phi) + w_{k+1} \cos(\phi) \\
 z_{k+1} &= z_k - u_{k+1} \cos(\phi) \cos(\xi) - v_{k+1} \sin(\xi) + w_{k+1} \sin(\phi) \cos(\xi)
 \end{aligned} \tag{8}$$

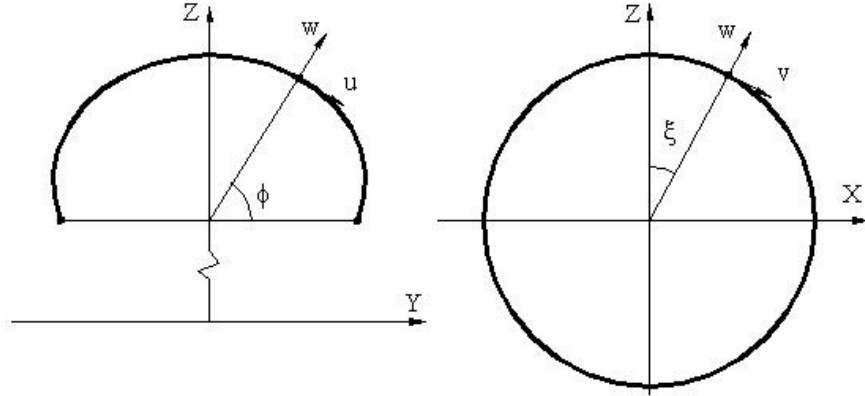


Figure 1: Displacement vectors u , v , and w

Results

There are two effective ways to determine the tire behavior, one is to apply external loads on the surface of the tire and determine the resultant deformations, and the other one is to use contact constrains for displacement and evaluate the force reactions. The pressure distribution in the contact area is strongly nonlinear having small values in the center of area and high values close to the limits of the contact area. An experimental set of data is required for the loads input case, while the second method is easier to apply and more efficient for this tire model.

The contact constrains are a new set of equations that are added to the general system of equations (7) by defining a value of displacement in Z direction.

$$Z_{def} - u_k \cos(\phi) \sin(\xi) + v_k \cos(\xi) + w_k \sin(\phi) \sin(\xi) = 0 \tag{9}$$

where Z_{def} is the iteration displacement, and u_k , v_k , and w_k are the corresponding deformations in the ϕ , ξ , and z direction.

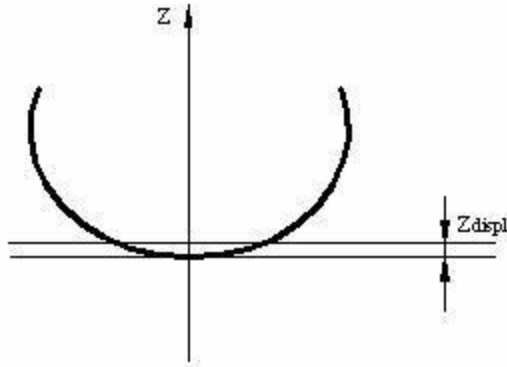


Figure 2: Contact constraint Z_{displ}

The number of contact constraint equations introduced is equal to the number of shells in contact with the ground. Additionally, an equal number of variables representing the normal load vector force on the shell elements are added to the matrix of variables.

The mesh size for this analysis is chosen to $61 \times 24 = 1464$ shell elements and the system of equations is composed of 4392 equations. The additional contact constraints will increase the number of equations to an average of 4410.

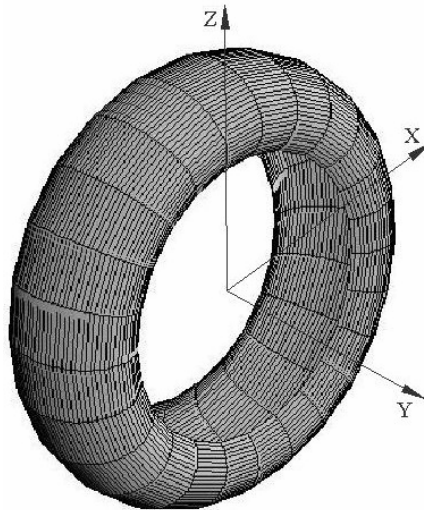


Figure 3: Tire Mesh of 1464 elements

Both the mesh size and the iteration step were chosen such that the accuracy of solutions is balanced by a reasonable computational time. The analysis has been performed on a Windows based machine with a Pentium 4 – 2.40 GHz processor. The average time for a complete run of one iteration step with Mathematica™ software was about 60 min, and 38 valid iterations were required to load the tire on a flat surface.

The algorithm for this simulation takes into consideration an important aspect of loading of the tire on a surface; in order to define a valid constraint, the resultant applied load has

to act as an external force and the resultant forces need to have the same sign [6]. If the constraints are not chosen properly, the iteration step has to be repeated at a different Z_{def} value. The total number of iterations performed was 60 with only 38 iterations valid.

Figure 4 represents the displacements u in the ϕ direction. The values are both positive and negative and show symmetry with respect to the crown of the tire.

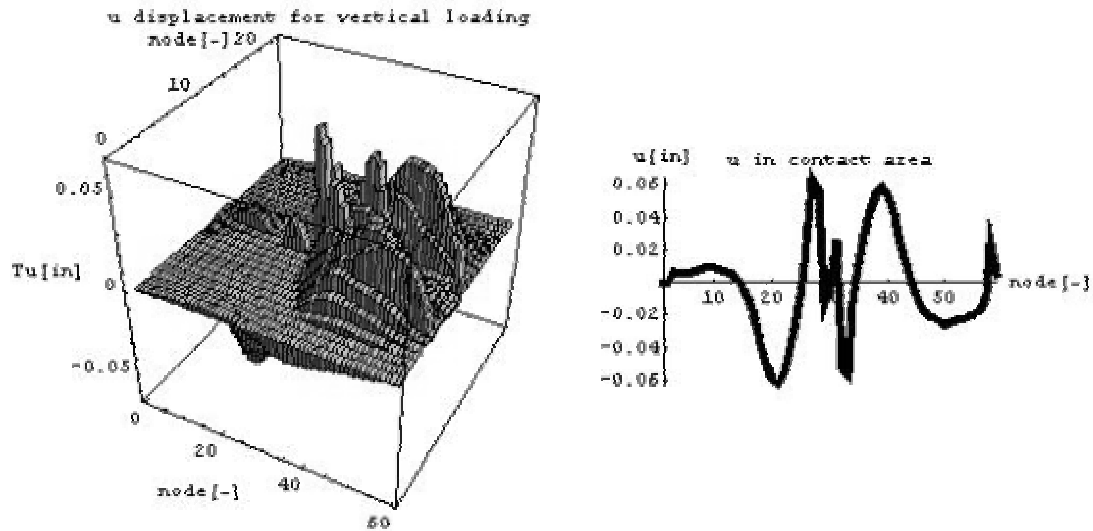


Figure 4: Displacement u for vertical loading

Displacement v in ξ direction has small values with maximum magnitude of 0.1 [in] as presented in Figure 5. The shape of the displacement plot and its values are as expected. At the contact region the displacements have higher values and slowly decay as the cross-sections are located at significant distance from the area. The maximum values computed for both ends of the contact cross section are the result of local rotations. The main reason for having rotations of the elements is the anisotropic properties of the structure. The longitudinal displacement has small influence on the cross-section profile.

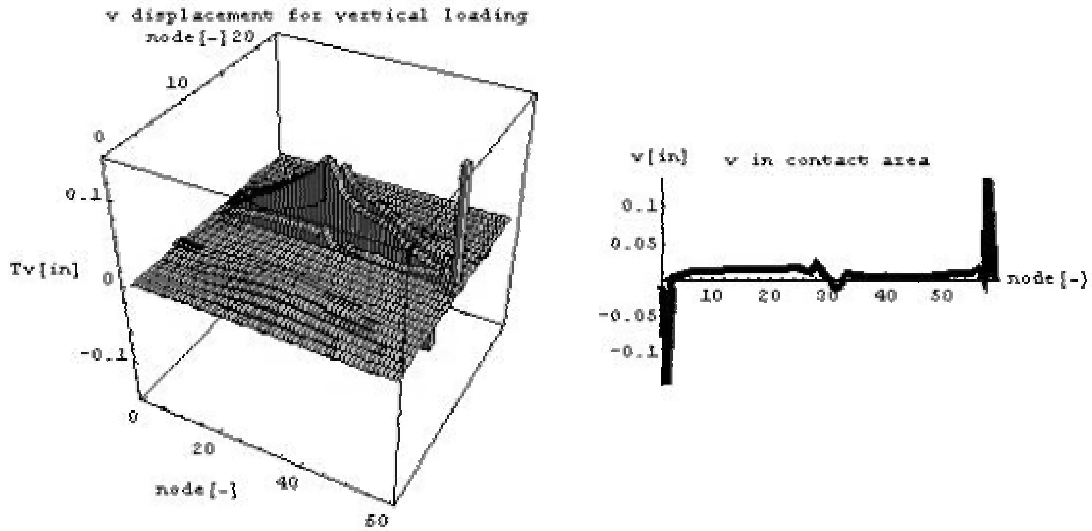


Figure 5: Displacement v for vertical loading

The normal displacement to the surface of the tire w is represented in Figure 6. Deformations are concentrated around the center of the contact area. Maximum value recorded along the profile is -0.562595 at the crown. The positive values between node 14-19 and 52-57 are a result of the expansion of the sidewall under deformation.

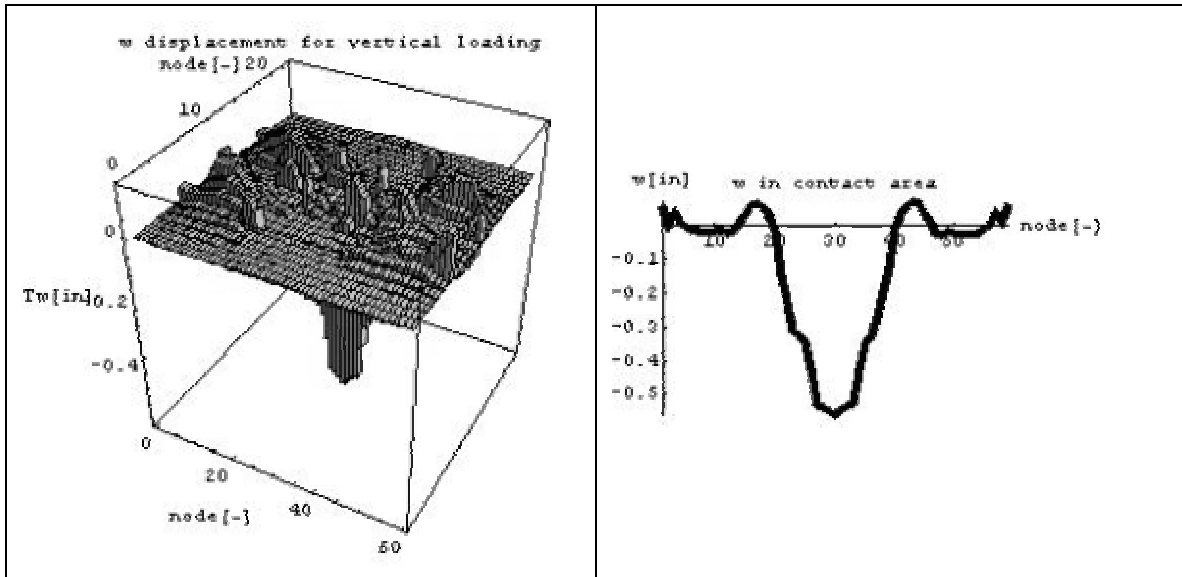


Figure 6: Displacement w for vertical loading

Using Equation (8), the deformed profile is computed after iteration. Figure 7 shows several iterations performed on the tire and give a combined view of the profile after inflation and the profile after vertical load is applied. The graphs represents iteration number 8, 18, 28, and the last iteration 38. While the crown follows the constraints, the

sidewall shows more deformations in the shoulder region, as expected. The sensitivity of the code to iteration step became significant after the 20th iteration, and a lower Δz deformation was required.

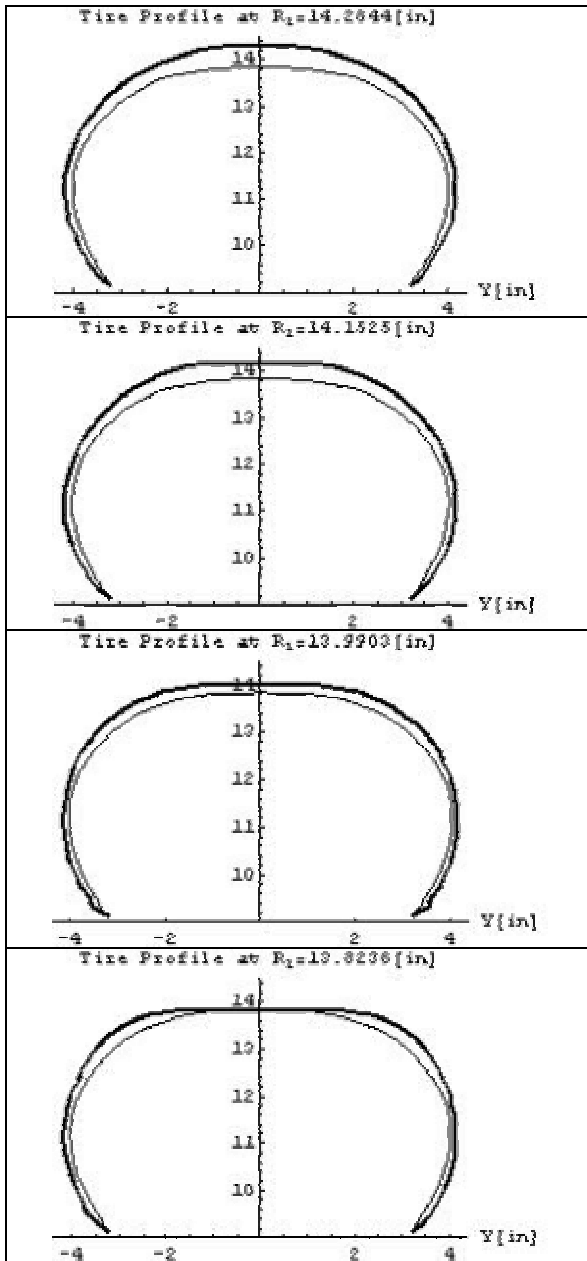


Figure 7: Cross-section deformed profile for vertical loading

The following table presents the loaded radius, the vertical deformation, and the maximum pressure applied on the shell elements in contact with the ground.

Iteration	z displacement	Max p_z [psi]
0	0	0
8	0.2343	7.84328
18	0.6006	86.8026
28	1.1289	160.568
38	1.8238	206.199

The actual load distribution in the contact area is presented in Figure 8. As expected, the distribution is variable with increased values towards the end limit of the area. During the iterations and progressive loading, the values of external load have a nonlinear distribution. Although the resolution of the output data is limited by the number of nodes chosen, the shape of the graphs are close to data presented in experimental reports [7].

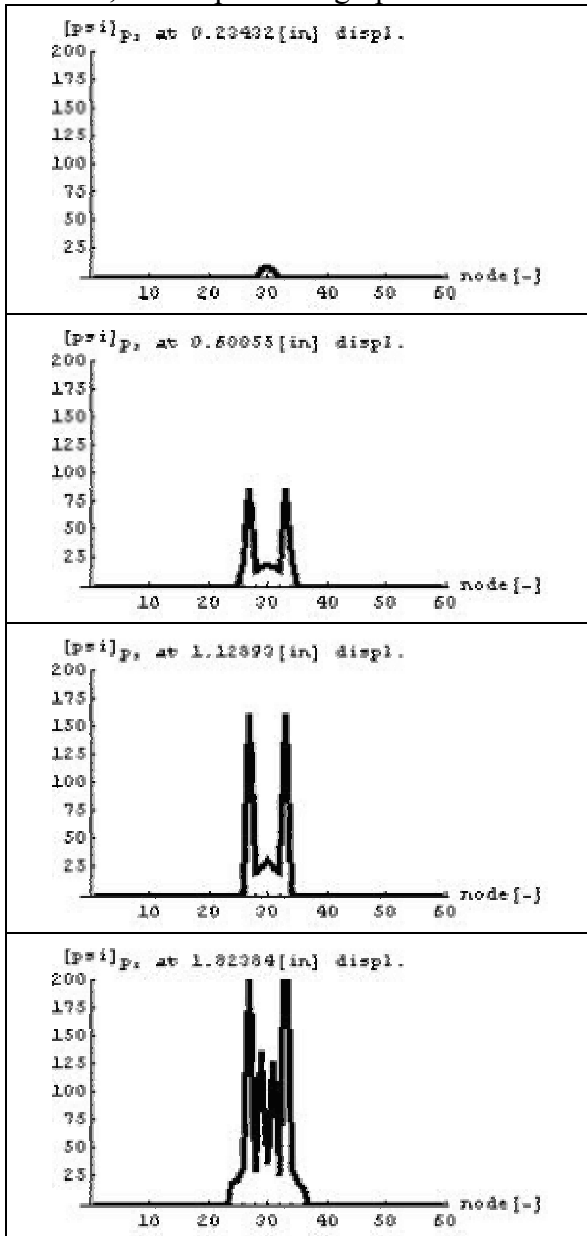


Figure 8: Pressure distribution in contact area

Conclusions

The recent developments of an advanced shell theory based tire model provide a framework for computation and simulation of tire-road interaction. Micro-mechanics, composite laminate theory, and shell theory are integrated in a consistent tire model solved by dual symbolic-numeric algorithm. Deformations, strains and moment resultants of the entire structure are described as function of structural material properties, undeformed tire profile, and applied forces.

The analysis was performed by applying local loads on the contact region between the tire and ground. The main advantage of performing a full analysis of the tire is that, beside deformations, the internal forces and moments are determined more accurately. The only significant limitation in the analysis was the computational power available at the time of the simulation. The code developed provides a convenient way to adjust the equations generation module based on the mesh size. Overall, the tire model advance the theoretical and computational developments to a new level and continue the research of analytical tire models in a continuum growing field of interest.

From a design point of view, the computer code is build with several modules well defined representing the compatibility, the constitutive and the equilibrium equations modules, finite difference scheme implementation, generation of equations, solver, and post-processing data module. One of the main advantages resulting from this tire model is the possibility of customizing for a wide variety of tire construction designs. Both radial and bias-ply types of tires are supported and detailed structural parameters are easily integrable in the tire model.

References

- [1] Bozdog, D., Olson, W. W., "An Advanced Shell Theory Based Tire Model", submitted for publication in Tire Science and Technology Journal, 2004.
- [2] Brewer, H. K., Stresses and Deformations in Multi-Ply Aircraft Tires Subject to Inflation Pressure Loading, Air Force Flight Dynamics Laboratory, Wright-Patterson Air Force Base, Ohio, 1970.
- [3] Vasiliev, V. V., Morozov, E. V., Mechanics and Analysis of Composite Materials, Elsevier, Netherlands, 2001.
- [4] Ventzel, E., Krauthammer, T., Thin Plates and Shells: Theory, Analysis, and Applications, Marcel Dekker, New York, 2001.
- [5] Walter, J. D., "Cord Reinforced Rubber," Chapter 3 of Mechanics of Pneumatic Tires, U.S. Department of Transportation, National Highway Traffic Safety Administration, D.C., 1981.

[6] Xu, Y., Jia, L., Zhang, J., “Modeling Tire/Road Contact Using Piecewise Ritz Procedure”, *Journal of Terramechanics* 42(2005) 99-113.

[7] El-Gindy, M., Lewis, H., “Development of a Tire/Pavement Contact-Stress Model Based on Artificial Neural Networks, Pub. FHWA-RD-99-041, Federal Highway Administration, 2001.